Optics Letters

High optical damage threshold on-chip lithium tantalate microdisk resonator

Xiongshuo Yan,[1,†] Yi'an Liu,[1,†] Licheng Ge,[1] Bing Zhu,[1] Jiangwei Wu,[1] Yuping Chen,[1,*] and Xianfeng Chen[1,2]

[1]State Key Laboratory of Advanced Optical Communication Systems and Networks, School of Physics and Astronomy, Shanghai Jiao Tong University, 800 Dongchuan Road, Shanghai 200240, China
[2]Collaborative Innovation Center of Light Manipulations and Applications, Shandong Normal University, Jinan 250358, China
*Corresponding author: ypchen@sjtu.edu.cn

Received 31 March 2020; revised 21 June 2020; accepted 21 June 2020; posted 22 June 2020 (Doc. ID 394171); published 16 July 2020

Lithium tantalate (LT) is one of the most attractive optical nonlinear materials, as it possesses a high optical damage threshold and great UV transparency (0.28–5.5 μm). Recently, optical grade LT nanoscale film was developed. Here a high-quality-factor (~ 10^5) LT microdisk resonator based on LT-on-insulator (LTOI) film is fabricated by utilizing focused ion beam (FIB) milling. 2 μW output second-harmonic waves are achieved in the LTOI microdisk at about 500 mW input power. Cascaded third-harmonic generation is also observed in the fabricated device. This work may pave the way for LTOI in integrated photonic chips.

https://doi.org/10.1364/OL.394171

Ferroelectric crystals such as lithium niobate ($LiNbO_3$, LN) [1–3], lithium tantalate ($LiTaO_3$, LT) [4,5] and potassium titanyl phosphate (KTP) [6] exhibit high practical utility in optical and photonic applications for their relatively large nonlinear coefficients and controllable domain structure. Especially for the LN industry, the technology revolution of LN-on-insulator (LNOI) gave birth to LN-substrate-based photonic integrated circuits in the past few years [3,7]. Ultrahigh-Q optical microcavities have important applications in fundamental physics and photonic integrated applications owing to their ability to strongly confine a light field [8–11]. Combining advantages of LN (low-loss transparency window, strong electro-optical coefficient, robustness [7]) and optical microcavities, LN microcavities have attracted much research interest and achieved many research findings in photonic integration [12–18]. However, there are some shortages for LN such as the low damage threshold and relatively narrow transparency range, which limit its application in high power light-input conditions especially for ultralhigh-Q microcavities and the mid-UV [19,20]. Luckily, LT possesses a higher optical damage threshold (i.e., laser-radiation-induced damage, 240 MW/cm^2 [21]) and greater UV transparency (0.28–5.5 μm) [4,22]. What is more, LT has relatively large nonlinear coefficents ($d_{33} \approx 26$ pm/v), and the other properties are also similar to LN [23,24]. It can be used widely in integrated photonic chips, especially in high input power fields. It should be noted that congruent LT (CLT) and near-stoichiometric LT (SLT) differ a lot in their properties [4,25,26]. Usually SLT has a lower coercive field, lower defect density, and higher photorefractive damage threshold than CLT. Doping magnesium oxide (MgO) in the crystal growth process can further improve the photorefractive damage threshold [20]. Conventional LT components are well studied, e.g., many methods are used to fabricate LT waveguides such as proton exchange [27], vapor diffusion [5], and femtosecond laser direct writing [28,29]. It is noted that to achieve efficient second- and third-harmonic waves in LT, periodically poled LT (PPLT) devices have been made [30], as well as periodically poled LN (PPLN) [31]. To simultaneously achieve efficient second- and third-harmonic (SH, TH, respectively) waves, quasiperiodic structure LT was designed [32]. What is more, an ultrahigh-Q LT resonator (~ 10^8) fabricated by mechanical polishing with diameters in the millimeter range and efficiently strong coupling has been achieved [24]. However, there is little research on smaller integrated LTOI microcavities, and their nonlinear properties have not been reported yet.

Here, a 50 μm diameter LTOI microdisk with a high Q-factor 2.67×10^5 is fabricated by using focused ion beam (FIB) milling [33] and is shown in Fig. 1(d). The high optical damage threshold of the LTOI microdisk is demonstrated. In addition, on-chip SH generation (SHG) and cascaded TH generation (THG) are also observed in the LTOI microdisk. Worthy of note is that further engineering of the domain structure for the phase-matching condition may move forward the nonlinear conversion efficiency [34].

The microdisk with a 50 μm diameter is fabricated on a Z-cut LTOI wafer shown in Fig. 1(a) which has a sandwich structure. The thicknesses of the CLT crystal and silica and silicon substrates are 600 nm, 2 μm, and 500 μm, respectively. In our fabrication process, first, the disk periphery is engineered precisely by using a scanning electron microscope (SEM) and FIB dual beam system (ZEISS Auriga), shown in Fig. 1(b). For a smoother sidewall, which contributes to the optical high-Q factor, we also choose a microring scanning pattern to remove residual the LT crystal from the edge of the disk. Then, the silica pedestal under the LT microdisk is formed by immersing in buffered oxide etching (BOE) solution, shown in Fig. 1(c).

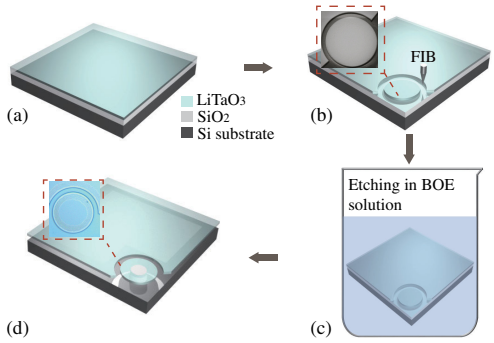

Fig. 1. LTOI sample and fabrication processing flow of an LTOI microdisk. (a) LTOI sample, (b) focused ion beam (FIB) milling and scanning electron microscope (SEM) image, (c) etching in buffered oxide etching (BOE) solution, and (d) LTOI microdisk with silica pedestal and optical microscope image.

Figure 1(d) shows the LT microdisk with a 2 μm thick pedestal. The inner most gray circle with a nearly round border is the top surface of the silica layer under LT film. This roundness is caused by the isotropic corrosion of silica by BOE solution acid. The outermost ring with a perfect round shape is the boundary of the LT microdisk.

Figure 2 shows the experimental setup for the characterization of the LTOI microdisk. A tunable continuous-wave laser (New Focus TLB-6728, linewidth < 200 kHz) is amplified by an erbium-doped fiber amplifier (EDFA) followed by a variable optical attenuator (VOA). Then we control the polarization of the input light by a polarization controller (PC). After this, we use a 2×2 50 : 50 single-mode fiber coupler for the wave splitting. On one path, the laser is launched into a tapered fiber to couple light into and out of the LTOI microdisk. We make the tapered fiber by the heating and pulling method. The waist diameter of the tapered fiber is approximately $1 \sim 2$ μm. On the other path, a power meter is used to monitor the input power simultaneously. In order to optimize the coupling efficiency and make an efficient nonlinear process a reality, the LTOI microdisk is placed on a precise 3D nanostage. Then we can change the input light polarization and adjust the contact point between the tapered fiber and the LTOI microdisk flexibly, which is related to coupling loss, to achieve high coupling efficiency. The transmitted light from the tapered fiber is then linked to another 2×2 90 : 10 fiber coupler. The 90% port of the fiber coupler is followed by an optical spectrum analyzer (OSA) to monitor the output spectrum. The 10% port is linked to an InGaAs photodetector (PD) and an oscilloscope (OSC) to monitor the transmission spectrum. What is more, the LTOI microdisk is monitored by an optical microscope (not shown in Fig. 2) from the top view.

To characterize the linear optical properties of the device, first, we shut down the EDFA and keep the optical power low enough to measure the transmission spectrum of the LTOI microdisk, in order to avoid interference from thermal effects. The transmission spectrum of the LTOI microdisk can be obtained by scanning the laser wavelength from 1535 nm to 1560 nm, which is shown in Fig. 3(a). The free spectral range (FSR) is measured around 7.2 nm, which is very close to the calculated FSR. The modes and polarization information were simulated by the finite element method (FEM). Figure 3(b) shows detailed characterizations of the whispering-gallery mode (WGM) with the center at 1544.24 nm, which is indicated by a black arrow in the transmission spectrum in Fig. 3(a). Fitting with a Lorentz function shows that the Q factor of the mode is measured to be 2.67×10^5, which is nearly on the same order compared to those obtained in other materials [35–37]. Of course, further optimization of the fabrication process can increase the Q factor to reach the same level as LN [38–40].

Nonlinear properties of the LTOI microdisk are also examined with greater pump laser intensity. We turn on the EDFA to amplify the seed laser and use the VOA to moderate the power appropriately. A coarse scan with the velocity of 0.1 nm/s is performed to search for the SHG. Once we observe SHG in the spectrometer, we record the pump light wavelength and do a fine scan with the velocity 0.01 nm/s to precisely lock the wavelength. The scattering light of SH collected by a CCD camera indicates that the light travels around the LTOI microdisk periphery and the measured spectrum of the SH signal at a wavelength of 773.68 nm, corresponding to a pump wavelength of 1547.36 nm, as shown in Fig. 4(a). FEM is used to calculate the fundamental wave (FW) and SH modes. We use indices n, m to denote radial and azimuthal mode numbers, respectively. The fundamental mode is $n = 1$, $m = 182$ ($FW_{1,182}$), while the SH mode is $n = 6$, $m = 364$ ($SH_{6,364}$, high-order mode), shown as the inset. The large refractive index difference between LT and air makes the light well confined and guarantees effective mode coupling. To confirm the SH signal is generated by second-order nonlinearity, we measure the relationship between SH signal and FW power. The SH signal power is collected from the tapered fiber output by OSA while the input power is measured by power meter (PM). We change the input pump power to collect the generated corresponding SH signal power. Figure 4(b) shows the quadratic dependence between the pump power and the SH signal power, well expected as a second-order nonlinear process. The cascaded THG is observed too. In this process, part

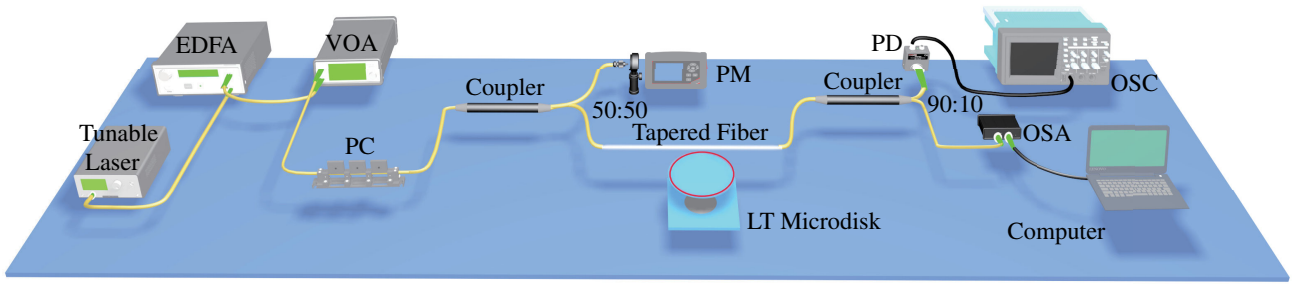

Fig. 2. Experimental setup for second nonlinear processes generating in LTOI microdisk. EDFA, erbium-doped fiber amplifier; VOA, variable optical attenuator; PC, polarization controller; PM, power meter; PD, photodetector; OSC, oscilloscope; OSA, optical spectrum analyzer.

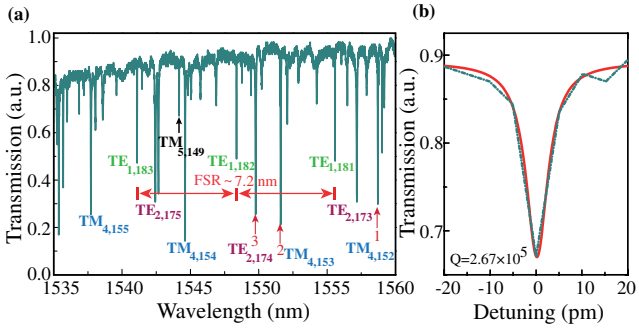

Fig. 3. (a) Transmission spectrum of a 50 μm diameter Z-cut LTOI microdisk in the telecommunication band. (b) Lorentzian fitting of a measured mode around 1544.24 nm indicated by a black arrow in (a), exhibiting a Q factor of 2.67×10^5.

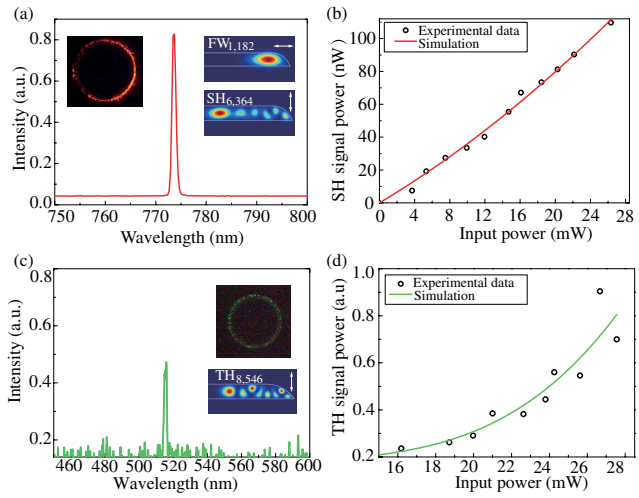

Fig. 4. (a) SH signal generated around 773.68 nm. Inset: optical image of scattered SH wave and simulated mode profile of the FW, SH waves. (b) Quadratic relationship of the SH power on the input FW power. (c) TH signal generated around 515.91 nm. Inset: optical image of scattered SH and TH waves and simulated mode profile of TH waves. (d) Cubic relationship of TH power on the input FW power. White arrow indicates polarization; horizontal arrow, TE; vertical arrow, TM.

of the SH power turns into the TH waves. Figure 4(c) shows the generated TH wave around 515.91 nm. The SH and TH waves scattered from the microdisk are observed as the upper inset image in Fig. 4(c). We also simulated the mode file of the TH wave, which corresponds to a high-order mode $TH_{8,546}$. Then, we calculated the effective indices of these three waves, which are $n_{\mathrm{eff,FW}}^{\mathrm{TE}} \approx 1.7940$, $n_{\mathrm{eff,SH}}^{\mathrm{TM}} \approx 1.7928$, and $n_{\mathrm{eff,TH}}^{\mathrm{TM}} \approx 1.7932$. From the effective indices of these three waves, we can find that the phase-matching conditions is met [18]. The cubic relationship between the TH power and the input FW power is achieved, as shown in Fig. 4(d). It is worth noting that considering the coupling loss and propagation loss, the actual nonlinear conversion efficiency should be higher. And if the SH couples from an individual bus waveguide, it will be more practical in real applications [41].

We all know that the optical energy in the cavity will reach its maximum at the critical coupling point. This can be evaluated

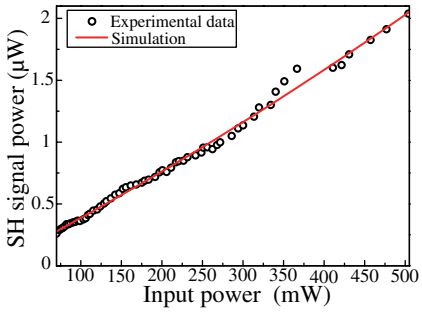

Fig. 5. Quadratic simulated relationship of SH power on high input FW power from 70 mW to 503 mW.

by the cavity buildup factor as [42]

$$\frac{P_{\mathrm{cav}}}{P_{\mathrm{in}}} = \frac{\lambda}{\pi^2 R n_{\mathrm{eff}}} Q_{\mathrm{ex}} \left(1 + \frac{Q_{\mathrm{ex}}}{Q_0}\right)^{-2}. \quad (1)$$

Here P_{cav} and P_{in} represent the intracavity power and coupled power, respectively. λ is the wavelength of the laser. R is the radius of the microcavity. n_{eff} is the effective refractive index of a certain optical mode. Q_{ex} and Q_0 are the external and intrinsic optical Q factors, respectively. From the equation, we can see that the circulating power in the microcavity is significantly enhanced. It means that a continuously high pump power may finally lead to the rupture of the microresonator. However, one of the important properties of LT is the high optical damage threshold. That means we can load more power into the LTOI microdisk.

Based on these advantages, in our experiment processes, we loaded the high input power from 70 mW to 503 mW in the LTOI microdisk, which did not damage it, and very high power SH waves were achieved. Figure 5 shows the quadratic relationship between the high input power and the SH power. We can see that our SH power can reach to 2 μW without any special phase-matching designs [12], under high input power. We also calculated the power density of the mode center when 503 mW input power was loaded into the LTOI microdisk, which was about 8.22×10^4 W/cm^2. It is worth pointing out that when we kept increasing the input power to 507 mW, the LTOI microdisk collapsed. At this point, the energy density in the cavity was about 8.28×10^4 W/cm^2. We suppose the optical damage threshold of LTOI is on the order of about 10^5 W/cm^2.

What is more, after investigating the nonlinear effects and optical damage threshold with high input power loaded, we remeasured the Q factor of the LTOI microdisk under the condition of low input power to avoid strong thermal and mechanical effects. In order to eliminate interference, we measured the modes 1, 2, and 3 shown in Fig. 3(a). The Q factors of these three modes are shown in Fig. (6), where (a), (b), and (c) correspond to the Q factor of modes 1, 2, and 3 before high power inputting and (d), (e), and (f) after high input power loading, respectively. Comparing these two sets of Q factors, we find that the Q factor has about an order of improvement on some modes. We think the reason could be that with the high input power and ultrahigh Q factor, there is a light-annealing-like process in the microdisk, which makes a smoother microdisk periphery [15]. It is worth stating that more details on the Q improvement still need further study.

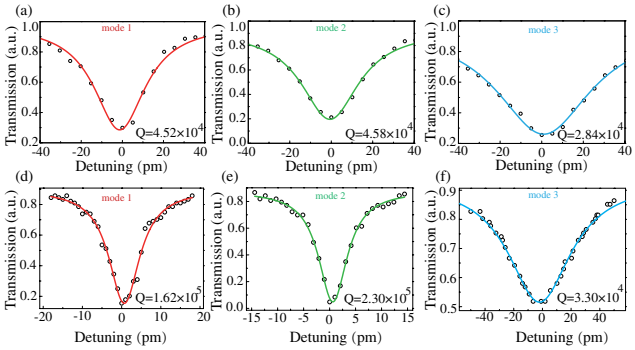

Fig. 6. (a)–(c) Q factors of modes 1, 2, and 3 in Fig. 3(a) before high input power loaded. (d)–(f) Q factors of modes 1, 2, and 3 after high input power loaded.

In summary, an on-chip LTOI microdisk with a high damage threshold and high Q factor (10^5) at the telecommunication band based on LTOI is fabricated by using the FIB milling method. Using the device, we have achieved SHG and cascading THG. The LTOI microdisk can be loaded with more than 500 mW input power without damaging it, making the SH power to reach the microwatt level (2 μW). What is more, we observed about an order of magnitude Q-factor improvement on some modes after high input power "annealing." We think photonic circuits will need to combine different materials and make use of their unique advantages [43]. LT with a high damage threshold and greater UV transparency can be an important material in photonic integration. It may play a more important role in future integrated photonic chips, especially in applications such as UV and high power functional devices.

Funding. National Key Research and Development Program of China (2017YFA0303700); National Natural Science Foundation of China (11574208, 91950107); Participation in Research Program of Shanghai Jiao Tong University (T072PRP34007).

Disclosures. The authors declare no conflicts of interest.

†These authors contributed equally to this Letter.

REFERENCES

1. R. Weis and T. Gaylord, Appl. Phys. A **37**, 191 (1985).
2. D. H. Jundt, Opt. Lett. **22**, 1553 (1997).
3. G. Poberaj, H. Hui, W. Sohler, and P. Guenter, Laser Photon. Rev. **6**, 488 (2012).
4. J.-P. Meyn and M. Fejer, Opt. Lett. **22**, 1214 (1997).
5. O. Eknoyan, D. Yoon, and H. Taylor, Appl. Phys. Lett. **51**, 384 (1987).
6. R. Le Targat, J.-J. Zondy, and P. Lemonde, Opt. Commun. **247**, 471 (2005).
7. A. Boes, B. Corcoran, L. Chang, J. Bowers, and A. Mitchell, Laser Photon. Rev. **12**, 1700256 (2018).
8. K. J. Vahala, Nature **424**, 839 (2003).
9. J.-H. Chen, X. Shen, S.-J. Tang, Q.-T. Cao, Q. Gong, and Y.-F. Xiao, Phys. Rev. Lett. **123**, 173902 (2019).
10. X. Zhang, Q.-T. Cao, Z. Wang, Y.-X. Liu, C.-W. Qiu, L. Yang, Q. Gong, and Y.-F. Xiao, Nat. Photonics **13**, 21 (2019).
11. A. Coillet, G. Lin, and Y. K. Chembo, Adv. Opt. Photon. **9**, 828 (2017).
12. J. Lin, N. Yao, Z. Hao, J. Zhang, W. Mao, M. Wang, W. Chu, R. Wu, Z. Fang, and L. Qiao, Phys. Rev. Lett. **122**, 173903 (2019).
13. M. Zhang, B. Buscaino, C. Wang, A. Shams-Ansari, C. Reimer, R. Zhu, J. M. Kahn, and M. Lončar, Nature **568**, 373 (2019).
14. H. Jiang, R. Luo, H. Liang, X. Chen, Y. Chen, and Q. Lin, Opt. Lett. **42**, 3267 (2017).
15. L. Ge, H. Jiang, Y. Liu, B. Zhu, C. Lu, Y. Chen, and X. Chen, Opt. Mater. Express **9**, 1632 (2019).
16. R. Luo, Y. He, H. Liang, M. Li, J. Ling, and Q. Lin, Phys. Rev. Appl. **11**, 034026 (2019).
17. R. Wolf, I. Breunig, H. Zappe, and K. Buse, Opt. Express **25**, 29927 (2017).
18. S. Liu, Y. Zheng, and X. Chen, Opt. Lett. **42**, 3626 (2017).
19. L. Wang, X. Zhang, L. Li, Q. Lu, C. Romero, J. R. V. de Aldana, and F. Chen, Opt. Express **27**, 2101 (2019).
20. K. Moutzouris, G. Hloupis, I. Stavrakas, D. Triantis, and M.-H. Chou, Opt. Mater. Express **1**, 458 (2011).
21. G. M. Zverev, E. Levchuk, V. A. Pashkov, and Y. D. Poryadin, Sov. J. Quantum Electron. **2**, 167 (1972).
22. A. Bruner, D. Eger, M. B. Oron, P. Blau, M. Katz, and S. Ruschin, Opt. Lett. **28**, 194 (2003).
23. S. Matsumoto, E. Lim, H. Hertz, and M. Fejer, Electron. Lett. **27**, 2040 (1991).
24. M. Soltani, V. Ilchenko, A. Matsko, A. Savchenkov, J. Schlafer, C. Ryan, and L. Maleki, Opt. Lett. **41**, 4375 (2016).
25. T. Hatanaka, K. Nakamura, T. Taniuchi, H. Ito, Y. Furukawa, and K. Kitamura, Opt. Lett. **25**, 651 (2000).
26. V. Y. Shur, E. Nikolaeva, E. Shishkin, A. Chernykh, K. Terabe, K. Kitamura, H. Ito, and K. Nakamura, Ferroelectrics **269**, 195 (2002).
27. P. J. Matthews, A. R. Mickelson, and S. W. Novak, J. Appl. Phys. **72**, 2562 (1992).
28. L. Li, W. Nie, Z. Li, B. Zhang, L. Wang, P. Haro-González, D. Jaque, J. R. V. de Aldana, and F. Chen, J. Lightwave Technol. **37**, 3452 (2019).
29. L. Wang, X. Zhang, L. Li, Q. Lu, C. Romero, J. R. V. de Aldana, and F. Chen, Opt. Express **27**, 2101 (2019).
30. Y. Liu, Z. Xie, W. Ling, Y. Yuan, X. Lv, J. Lu, X. Hu, G. Zhao, and S. Zhu, Opt. Express **19**, 17500 (2011).
31. M. Hu, Y. Chen, G. Li, and X. Chen, Chin. Opt. Lett. **14**, 61301 (2016).
32. S. Zhu, Y. Zhu, and N. Ming, Science **278**, 843 (1997).
33. J. Lin, Y. Xu, Z. Fang, M. Wang, J. Song, N. Wang, L. Qiao, W. Fang, and Y. Cheng, Sci. Rep. **5**, 8072 (2015).
34. I. Breunig, Laser Photon. Rev. **10**, 569 (2016).
35. S. Mariani, A. Andronico, O. Mauguin, A. Lematre, I. Favero, S. Ducci, and G. Leo, Opt. Lett. **38**, 3965 (2013).
36. P. S. Kuo, J. Bravo-Abad, and G. S. Solomon, Nat. Commun. **5**, 3109 (2014).
37. D. P. Lake, M. Mitchell, H. Jayakumar, L. F. dos Santos, D. Curic, and P. E. Barclay, Appl. Phys. Lett. **108**, 031109 (2016).
38. M. Zhang, C. Wang, R. Cheng, A. Shams-Ansari, and M. Lončar, Optica **4**, 1536 (2017).
39. Y. He, H. Liang, R. Luo, M. Li, and Q. Lin, Opt. Express **26**, 16315 (2018).
40. R. Wu, J. Zhang, N. Yao, W. Fang, L. Qiao, Z. Chai, J. Lin, and Y. Cheng, Opt. Lett. **43**, 4116 (2018).
41. X. Guo, C.-L. Zou, and H. X. Tang, Optica **3**, 1126 (2016).
42. T. J. A. Kippenberg, "Nonlinear optics in ultra-high-Q whispering-gallery optical microcavities," Ph.D. thesis (California Institute of Technology, 2004).
43. L. Chang, M. H. Pfeiffer, N. Volet, M. Zervas, J. D. Peters, C. L. Manganelli, E. J. Stanton, Y. Li, T. J. Kippenberg, and J. E. Bowers, Opt. Lett. **42**, 803 (2017).